

Efficient and controlled symmetric and asymmetric Bell-state transfers in a dissipative Jaynes-Cummings model

Qi-Cheng Wu(吴奇成), Yu-Liang Fang(方玉亮), Yan-Hui Zhou(周彦辉), Jun-Long Zhao(赵军龙), Yi-Hao Kang(康逸豪), Qi-Ping Su(苏奇平), and Chui-Ping Yang(杨垂平)

Citation: Chin. Phys. B, 2026, 35 (**1**): 010304. DOI: 10.1088/1674-1056/ae111f
http://cpb.iphy.ac.cn; http://iopscience.iop.org/cpb

What follows is a list of articles you may be interested in

Exceptional rings and non-Abelian topology in non-Hermitian high-spin systems

Peng-Zhen Sun(孙鹏震), Zhou-Tao Lei(雷周涛), and Yuan-Gang Deng(邓元刚)
Chin. Phys. B, 2025, 34 (**11**): 110303. DOI: 10.1088/1674-1056/addcbe

Non-quantized Zak phases, PT/APT symmetry transitions, and doubly degenerate exceptional points in a non-Hermitian spin-orbit coupled SSH model

Jun-Xing Huo(霍俊行), Jian Li(李健), Qing-Xu Li(李清旭), and Jia-Ji Zhu(朱家骥)
Chin. Phys. B, 2025, 34 (**7**): 070301. DOI: 10.1088/1674-1056/adc7f3

Exceptional points and quantum dynamics in a non-Hermitian two-qubit system

Yi-Xi Zhang(张益玺), Zhen-Tao Zhang(张振涛), Zhen-Shan Yang(杨震山), Xiao-Zhi Wei(魏晓志), and Bao-Long Liang(梁宝龙)
Chin. Phys. B, 2024, 33 (**6**): 060308. DOI: 10.1088/1674-1056/ad2a70

Topological properties of non-Hermitian Creutz ladders

Hui-Qiang Liang(梁辉强) and Linhu Li(李林虎)
Chin. Phys. B, 2022, 31 (**1**): 010310. DOI: 10.1088/1674-1056/ac3991

Two-body exceptional points in open dissipative systems

Peize Ding(丁霈泽) and Wei Yi(易为)
Chin. Phys. B, 2022, 31 (**1**): 010309. DOI: 10.1088/1674-1056/ac3396

RAPID COMMUNICATION

Efficient and controlled symmetric and asymmetric Bell-state transfers in a dissipative Jaynes–Cummings model

Qi-Cheng Wu(吴奇成)[1,†,‡], Yu-Liang Fang(方玉亮)[1,†], Yan-Hui Zhou(周彦辉)[1], Jun-Long Zhao(赵军龙)[1], Yi-Hao Kang(康逸豪)[2], Qi-Ping Su(苏奇平)[2], and Chui-Ping Yang(杨垂平)[2,§]

[1] *Quantum Information Research Center and Jiangxi Province Key Laboratory of Applied Optical Technology, Shangrao Normal University, Shangrao* 334001, *China*

[2] *School of Physics, Hangzhou Normal University, Hangzhou* 311121, *China*

(Received 9 September 2025; revised manuscript received 30 September 2025; accepted manuscript online 9 October 2025)

Realizing efficient and controlled state transfers is necessary for implementing a wide range of classical and quantum information protocols. Recent studies have demonstrated that both asymmetric and symmetric state transfers can be achieved by encircling an exceptional point (EP) in non-Hermitian (NH) systems. However, the application of this phenomenon has been restricted to scenarios where an EP exists in single-qubit systems and is associated with a specific type of dissipation. In this work, we demonstrate efficient and controlled symmetric and asymmetric Bell-state transfers by modulating system parameters within a Jaynes–Cummings model while accounting for atomic spontaneous emission and cavity decay. The effective suppression of nonadiabatic transitions enables a symmetric exchange of Bell states irrespective of the encircling direction. Furthermore, we report a counterintuitive finding: the presence of an EP is not indispensable for implementing asymmetric state transfers in NH systems. We achieve perfect asymmetric Bell-state transfers even in the absence of an EP by dynamically orbiting around an approximate EP. Our work presents an approach to effectively and reliably manipulate entangled states with both symmetric and asymmetric characteristics, through dissipation engineering in NH systems.

Keywords: exceptional points, adiabatic Bell-state transfer, chiral Bell-state transfer, Jaynes–Cummings model

PACS: 03.67.–a, 42.50.Dv, 74.40.Kb

DOI: 10.1088/1674-1056/ae111f **CSTR:** 32038.14.CPB.ae111f

1. Introduction

Since the discovery of exceptional points (EPs),[1–6] a plethora of counterintuitive phenomena have emerged in non-Hermitian (NH) systems,[7–14] encompassing heightened sensitivity to perturbations,[15–17] loss-induced transparency effects,[18,19] and the existence of distinctive topological structures.[20,21] Recent studies have also revealed that symmetric (adiabatic) state transfer[21–23] and asymmetric (chiral) state transfer[24–34] can be accomplished by adjusting system parameters along a path encircling an exceptional point (EP). In general, the symmetric transfer between the eigenstates of a system implies that the state transfer is solely determined by the initial state and remains unaffected by the encircling direction. Conversely, the asymmetric transfer between the system eigenstates indicates that the state transfer is solely determined by the encircling direction. The discoveries and applications of symmetric and asymmetric state transfers in time-modulated NH systems have undoubtedly made significant contributions to advancements in the quantum field.[22–24,33–36]

However, it is regrettable that the existing research[21–36] predominantly focuses on either symmetric or asymmetric state transfer, with limited exploration of the simultaneous involvement of both types or mode conversion between the two within the same quantum system. Furthermore, current schemes for state transfer and their underlying protocols critically rely on the presence of EPs, requiring specific designs of non-Hermitian effective Hamiltonians with finely tuned parameters. Moreover, these schemes also impose constraints primarily associated with dissipation, typically considering only a single type, such as spontaneous radiation dissipation or cavity decay,[22,23,37,38] which differs from real-world scenarios, where quantum systems often experience multiple forms of dissipation. Finally, while achieving successful demonstrations of symmetric or asymmetric state transfer in single-bit systems is noteworthy, efficiently accomplishing entangled state transfers (i.e., Bell states[39–41]) in systems with multiple types of dissipation remains a challenging task.

In this work, we demonstrate efficient and controlled symmetric and asymmetric Bell-state transfers through mod-

[†]These authors contributed equally to this work.

[‡]Corresponding author. E-mail: wuqi.cheng@163.com

[§]Corresponding author. E-mail: yangcp@hznu.edu.cn

© 2026 Chinese Physical Society and IOP Publishing Ltd. All rights, including for text and data mining, AI training, and similar technologies, are reserved.

ulation of system parameters in a Jaynes–Cummings model with both atomic spontaneous emission and cavity decay. We effectively mitigate the influence of nonadiabatic transitions induced by the imaginary component of the eigenenergy spectrum through appropriate parameter configurations. Subsequently, by selecting a trajectory that dynamically encircles an EP, we successfully realize a long-desired symmetric Bell-state transfer, wherein the exchange of Bell states occurs dynamically irrespective of the encircling direction. Moreover, we present a counterintuitive finding, which suggests that the presence of an EP may not be indispensable for the successful implementation of asymmetric state transfer in NH systems. Furthermore, we achieve perfect asymmetric Bell-state transfers even in the absence of an EP while dynamically orbiting around an approximate exceptional point (AEP). Finally, we demonstrate that our results hold for the Jaynes–Cummings model under time-modulated and time-independent dissipation, where the final Bell-state transfer is determined by the trajectory orientation. Our work presents a novel approach for effectively and reliably manipulating entangled states with both symmetric and asymmetric characteristics through dissipation engineering in NH systems.

The rest of this paper is organized as follows. In Section 2, we provide a concise overview of the dissipative Jaynes–Cummings model. Sections 3 and 4 are dedicated to detailed analyses of the energy spectrum and eigenstate population distribution for symmetric and asymmetric Bell-state transfer, respectively. Finally, we present the experimental feasibility and summary in Section 5.

2. Dissipative Jaynes–Cummings model

As shown in Fig. 1, we consider a dissipative Jaynes–Cummings model, in which a two-level atom (with the ground state $|g\rangle$ and the excited state $|e\rangle$) is coupled to a single-mode cavity with coupling strength g. The decay rate of the cavity mode and the atomic spontaneous emission rate are respectively indicated by κ and γ. Generally, the dynamics of the dissipative Jaynes–Cummings model obey the following Markovian master equation[42,43] (taking $\hbar = 1$):

$$\begin{aligned}\dot{\rho} &= -\mathrm{i}[H_0(t),\rho]+\mathcal{L}(\rho),\\ H_0 &= \omega_a a^\dagger a+\omega_e\sigma_+\sigma_-+g(a^\dagger\sigma_-+a\sigma_+),\\ \mathcal{L}(\rho) &= \kappa\left(a\rho a^\dagger-\frac{1}{2}\{a^\dagger a,\rho\}\right)\\ &\quad+\gamma\left(\sigma_-\rho\sigma_+-\frac{1}{2}\{\sigma_+\sigma_-,\rho\}\right),\end{aligned} \tag{1}$$

where ω_a is the cavity resonance frequency, while ω_e is the transition frequency between the two levels $|g\rangle$ and $|e\rangle$ of the atom. The creation (annihilation) operator of the cavity mode is denoted as $a^\dagger$ (a), and the raising (lowering) operator of the atom is represented by σ_+ (σ_-). It should be noted that the effects of the so-called quantum jump terms, $\gamma\sigma_-\rho\sigma_+$ and $\kappa a\rho a^\dagger$, can be neglected when the decay rate of the cavity mode (κ) and the atomic spontaneous emission rate (γ) are very small, or when cavity decay and atomic spontaneous emission are experimentally measured via postselection protocols.[44,45] In those cases, the effective Hamiltonian describing this system can be expressed as follows:[46,47]

$$H_{\mathrm{eff}} = H_0-\frac{\mathrm{i}\kappa}{2}a^\dagger a-\frac{\mathrm{i}\gamma}{2}\sigma_+\sigma_-. \tag{2}$$

In the absence of an additional driving field, we make the reasonable assumption that the total excitation of the system is unity.[46,48–51] We denote the vacuum state (the single-photon state) of the cavity as $|0\rangle$ ($|1\rangle$). In the basis states $|e,0\rangle = |1,0\rangle^{\mathrm{T}}$ and $|g,1\rangle = |0,1\rangle^{\mathrm{T}}$, where T stands for transpose, the effective Hamiltonian can be expressed as

$$H^1_{\mathrm{eff}} = \begin{pmatrix}\omega_a+\delta-\frac{\mathrm{i}\gamma}{2} & g\\ g & \omega_a-\frac{\mathrm{i}\kappa}{2}\end{pmatrix}, \tag{3}$$

where $\delta = \omega_e-\omega_a$ is the difference between the atomic transition frequency and the cavity frequency. The eigenvalues of the NH Hamiltonian (H^1_{eff}) are

$$\begin{aligned}E_\pm &= \frac{1}{4}[2(2\omega_a+\delta)-\mathrm{i}(\gamma+\kappa)\pm 2\Delta_E],\\ \Delta_E &= \frac{\mathrm{i}}{2}\sqrt{(\gamma-\kappa+2\mathrm{i}\delta)^2-16g^2},\end{aligned} \tag{4}$$

and the corresponding right eigenvectors are

$$|\phi_\pm\rangle = \frac{1}{S_\pm}[A_\pm,4g]^{\mathrm{T}}, \tag{5}$$

where $A_\pm = 2\delta-\mathrm{i}(\gamma-\kappa)\pm 2\Delta_E$ and $S_\pm = \sqrt{|A_\pm|^2+|4g|^2}$, together with the left eigenvectors

$$\langle\widehat{\phi_\pm}| = \frac{1}{S_\pm}[A_\pm,4g]. \tag{6}$$

The biorthogonal partners $\{\langle\widehat{\phi_n}|\}$ and $\{|\phi_m\rangle\}$ $(n,m=+,-)$ are normalized to satisfy the biorthogonality relations $\langle\widehat{\phi_n}|\phi_m\rangle = \delta_{nm}$ and $\sum_n|\widehat{\phi_n}\rangle\langle\phi_n| = \sum_n|\phi_n\rangle\langle\widehat{\phi_n}| = 1$.[10]

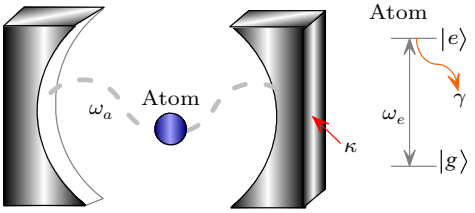


Fig. 1. Schematic illustration of a dissipative Jaynes–Cummings model for a hybrid atom–cavity system. Here, ω_a denotes the cavity resonance frequency, and ω_e is the transition frequency between the atomic ground state $|g\rangle$ and excited state $|e\rangle$. The parameters κ and γ represent the decay rate of the cavity mode and the atomic spontaneous emission rate, respectively.

The difference $\Delta_E(\delta,g,\gamma,\kappa)$ between the eigenvalues ($E_\pm$) plays a pivotal role in determining the eigenenergy spectrum and the system dynamics. However, analyzing the relationship between all four parameters (δ,g,γ,κ) and Δ_E simultaneously presents a significant challenge. Therefore, it is convenient to fix certain parameters and thoroughly investigate the correlation between the remaining parameters and Δ_E. This step is crucial for identifying EPs within the system. Once the EPs are determined, the primary objective is to design a time-evolution trajectory that encompasses the EPs in order to achieve asymmetric or symmetric Bell-state transfer. In this context, we provide several remarks regarding the design of the time-evolution trajectory. (i) It is crucial to ensure that the eigenvectors $|\phi_+\rangle$ and $|\phi_-\rangle$ correspond to Bell states $(|1,0\rangle \pm |0,1\rangle)/\sqrt{2}$ at both the beginning and end of the trajectory. To ensure the formation of Bell states, it is necessary to maintain $\delta_{t_\mathrm{i},t_\mathrm{f}} = (\gamma-\kappa)_{t_\mathrm{i},t_\mathrm{f}} = 0$ [where t_i (t_f) represents the initial (final) time], such that $|\phi_+(t_\mathrm{i},t_\mathrm{f})\rangle$ and $|\phi_-(t_\mathrm{i},t_\mathrm{f})\rangle$ become Bell states. (ii) Both the real and imaginary components of the time-evolution trajectory should be carefully designed to encircle or closely approach the EP. The subsequent sections are devoted to the exploration of appropriate time-evolution trajectories for achieving symmetric and asymmetric Bell-state transfers.

3. Symmetric Bell-state transfer

Recent studies[21–23] have demonstrated that achieving efficient symmetric state transfer hinges on satisfying the generalized adiabatic condition

$$\sum_{n\neq m} \frac{\left|\langle\widehat{\phi}_n(t)|\dot{\phi}_m(t)\rangle\right|}{|\omega_{nm}(t)|} \exp\left(\mathrm{i}\int_0^t \omega_{nm}(\tau)\,\mathrm{d}\tau\right) \ll 1, \tag{7}$$

where $\omega_{nm}(t) = E_m(t) - E_n(t)$ represents the difference between the corresponding eigenvalues of $H(t)$, and $\langle\widehat{\phi}_n(t)|\dot{\phi}_m(t)\rangle$ quantifies the nonadiabatic coupling between instantaneous eigenstates. It is worth noting that in NH systems, the eigenvalues are generally complex. The exponential factor involving the imaginary part of $\omega_{nm}(t)$, given by $\exp(-\mathrm{Im}(\omega_{nm}(t)))$, can induce either damping or amplification of the evolving state. Even a small eigenvalue difference can lead to significant dynamical effects when the adiabatic evolution trajectory approaches an EP. Furthermore, nonadiabatic couplings become more pronounced as the rate of system evolution increases in the absence of external control.

Inspired by the ideas presented in Refs. [21–23], in this section we propose a controlled scheme to realize a long-sought symmetric Bell-state transfer, in which the transfer occurs dynamically and independently of the encircling direction. This is achieved by slowing down the system evolution and minimizing the imaginary component $\mathrm{Im}(\Delta_E(\delta,g,\gamma,\kappa))$. Specifically, the imaginary component $\mathrm{Im}(\Delta_E(\delta,g,\gamma,\kappa))$ can be effectively eliminated by adopting appropriate parameter configurations, such as $\delta = 0$ and $16g^2 > (\gamma-\kappa)^2$. For the purpose of discussion, we assume $\kappa = \alpha\gamma$ and normalize all parameters with respect to the cavity frequency ω_a in the subsequent analysis.

Based on the aforementioned settings, we can investigate the intricate correlation between the energy difference and the remaining two parameters (g,γ) in a three-dimensional context. In order to gain an intuitive understanding of the energy variation within the system, in Fig. 2, we illustrate the eigenenergy spectrum $E_\pm$ in the parameter space (g,γ). From Fig. 2, it is evident that the imaginary parts of E_+ and E_- intersect with the plane defined by $E = 0$, while their real counterparts intersect with another plane characterized by $E = 1$. The intersection point of these two planes within the parameter space (g,γ) corresponds to a pink point at coordinates $(0,0)$, which represents an EP. Consequently, by steering the system evolution trajectory around or in close proximity to this EP, we can achieve a symmetric transfer of Bell states as desired.

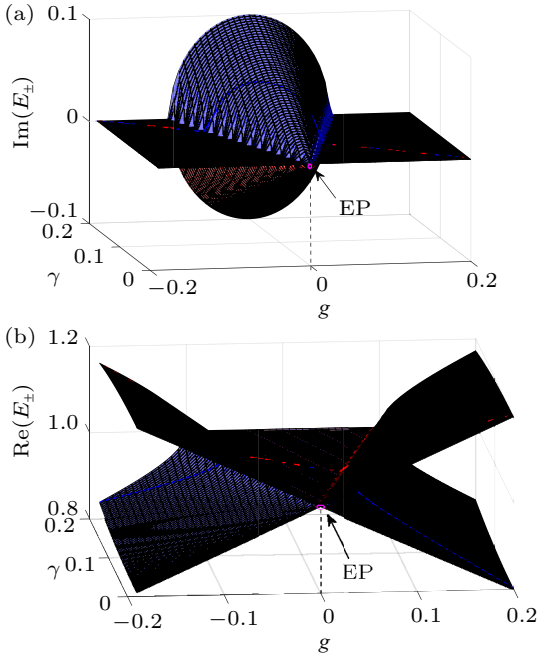


Fig. 2. The eigenenergy spectrum $E_\pm(g,\gamma)$ and the system time-evolution trajectory $E_\pm[g(t),\gamma(t)]$ for symmetric Bell-state transfer. Panels (a) and (b) show the imaginary and real parts of $E_\pm(g,\gamma)$ and $E_\pm[g(t),\gamma(t)]$, respectively. The blue (red) Riemann surface corresponds to $E_+(g,\gamma)$ [$E_-(g,\gamma)$], while the dashed blue (solid red) line represents $E_+[g(t),\gamma(t)]$ ($E_-[g(t),\gamma(t)]$), respectively. The pink point denotes an exceptional point (EP). The other parameters are chosen as $g_0 = 0.01$, $G_0 = \Gamma_0 = 0.2$, $\alpha = -1$, and $\omega = \pi$.

A symmetric Bell-state transfer can be realized through the careful selection of the parameter trajectory

$$g(t) = g_0 + G_0\cos(\omega t), \quad \gamma(t) = \Gamma_0\sin^2(\omega t), \tag{8}$$

where g_0, G_0, Γ_0, and ω are real constants. Without loss of generality, we consider the following parameter selection:

$g_0 = 0.01$, $G_0 = \Gamma_0 = 0.2$, $\alpha = -1$, and $\omega = \pi$. Subsequently, Fig. 2 depicts the time-evolution trajectories. In this figure, the dashed blue line represents $E_+[g(t), \gamma(t)]$, while the solid red line corresponds to $E_-[g(t), \gamma(t)]$. It is evident that both trajectories revolve around the pink exceptional point (EP), consistent with our assumptions. Moreover, based on Eq. (8), the non-Hermitian (NH) Hamiltonian $H^1_{\rm eff}(t)$ exhibits periodic variations as a function of time t, with a period $T = \pi/\omega$.

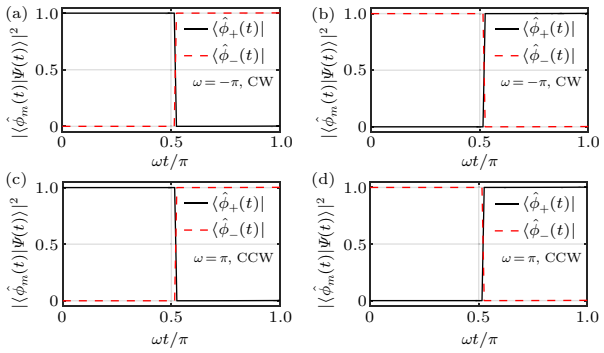


Fig. 3. Time evolution of the fidelity $F_m = |\langle\widehat{\phi_m}(t)|\Psi(t)\rangle|^2$ for the time-dependent right eigenstate $|\phi_m(t)\rangle$ $(m = +, -)$. The initial state in panels (a) and (c) [(b) and (d)] is chosen as $|\Psi(0)\rangle = |\phi_+(0)\rangle$ ($|\phi_-(0)\rangle$). The trajectory direction in panels (a)–(b) is clockwise (CW) and in panels (c)–(d) is counterclockwise (CCW). The other parameters are $g_0 = 0.01$, $G_0 = \Gamma_0 = 0.2$, and $\alpha = -1$. The state dynamics exhibits a purely adiabatic character, enabling the implementation of a symmetric Bell-state switch.

To evaluate the validity of the symmetric Bell-state transfer, we investigate the system dynamics. The fidelity of the right eigenstate $|\phi_m(t)\rangle$ $(m = +, -)$ is determined by the relation $F_m = |\langle\widehat{\phi_m}(t)|\Psi(t)\rangle|^2$, where $|\Psi(t)\rangle$ represents the evolving state of the system at time t. Assuming that the system is initially prepared in one of its right eigenstates, i.e., $|\Psi(0)\rangle = |\phi_\pm(0)\rangle = (|e,0\rangle \pm |g,1\rangle)/\sqrt{2}$, we numerically integrate Schrödinger's equation

$$\mathrm{i}\partial_t|\Psi(t)\rangle = H^1_{\rm eff}(t)|\Psi(t)\rangle, \tag{9}$$

to obtain the evolving state $|\Psi(t)\rangle$. The instantaneous left eigenvector $\langle\widehat{\phi_m}(t)|$ can be calculated by substituting the parameters into Eqs. (6) and (8). The results of these calculations for different encircling directions and initial states are illustrated in Fig. 3. Figures 3(a)–3(d) demonstrate complete Bell-state transfers (achieving maximal transfer fidelity of 1 by employing sufficiently slow trajectories), where $|\phi_-(t)\rangle \leftrightarrow |\phi_+(t)\rangle$ are exchanged after one period $T = \pi/\omega$, irrespective of the encircling direction. In this context, the state evolution exhibits distinct adiabatic characteristics, enabling the realization of symmetric Bell-state switching. Furthermore, it is evident that the state vectors undergo a rapid transition near $\omega t = \pi/2$, in agreement with predictions reported in Refs. [22,23]. This phenomenon can be attributed to the mechanism of nonadiabatic coupling transitions between eigenstates in non-Hermitian systems and the influence of pseudo-Hermiticity. On one hand, as demonstrated in Ref. [23], the nonadiabatic coupling transition between eigenstates exhibits exponential growth with respect to the imaginary part of the system eigenvalue difference Δ_E. More specifically, the larger the imaginary component of the eigenvalue difference, the more pronounced the nonadiabatic coupling transition becomes. Based on Eqs. (4) and (8), it is clear that the extremum of the system eigenvalue difference Δ_E occurs at half of the period ($\omega t = \pi/2$), thereby inducing a significant nonadiabatic coupling transition at $\omega t = \pi/2$. On the other hand, pseudo-Hermiticity (most prominent when $\delta = 0$, $g_0 = 0$, and $\alpha = -1$) generates symmetric system dynamics during the first and second halves of the period. Theoretically, when the system simultaneously satisfies conditions for strong nonadiabatic coupling transitions and pseudo-Hermiticity, the state vectors undergo a rapid transition precisely at $\omega t = \pi/2$. However, this theoretical prediction slightly differs from the results presented in Fig. 3, which can be attributed to the imperfect realization of pseudo-Hermiticity (e.g., $\delta = 0$, $g_0 = 0.01$, and $\alpha = -1$).

4. Asymmetric Bell-state transfer

4.1. Asymmetric Bell-state transfer under time-modulated dissipation

In this subsection, we propose a controlled scheme to realize asymmetric Bell-state transfer. Specifically, we begin by fixing the value of g and systematically analyzing the relationship between the energy difference and the parameters (δ, γ). It is important to note that the intersection surface of the intrinsic energy spectrum plays a crucial role in scheme design. This is because, in general, the successful transfer of asymmetric or chiral states critically depends on the topological properties of the intersecting Riemann energy manifolds at EPs.[24–32] For clarity, we define the diabolic line (D line) and the L-shaped curve (L line) as the intersection lines of the surfaces corresponding to the imaginary and real parts of the eigenenergy spectrum $E_\pm(\gamma, \delta)$, respectively.

As illustrated in Fig. 4, we present a graphical depiction of the eigenenergy spectrum $E_\pm$ in the parameter space (δ, γ). Figures 4(a) and 4(b) respectively display the three-dimensional variations of the imaginary and real parts of the eigenenergy spectrum $E_\pm(\gamma, \delta)$, as well as the time-evolution trajectory $E_\pm[\gamma(t), \delta(t)]$. Furthermore, Figs. 4(a) and 4(c) reveal that the imaginary components of $E_+(\gamma, \delta)$ and $E_-(\gamma, \delta)$ intersect along the diabolic line (D line), where $\mathrm{Im}(E_+) = \mathrm{Im}(E_-) = 0$ (see the yellow line in Figs. 4(a), 4(c), and 4(d)). Meanwhile, Figs. 4(b) and 4(d) show that the real components of $E_+(\gamma, \delta)$ and $E_-(\gamma, \delta)$ converge along an L-shaped curve (L line), corresponding to $\mathrm{Re}(E_+) = \mathrm{Re}(E_-) = 1$ (see the cyan L-shaped line in Fig. 4(d)). Furthermore, by comparing Figs. 4(c) and 4(d), it becomes apparent that the imag-

inary and real parts of the spectrum $E_{\pm}(\gamma,\delta)$ cannot coincide simultaneously [$\mathrm{Im}(E_+)=\mathrm{Im}(E_-)$ and $\mathrm{Re}(E_+)=\mathrm{Re}(E_-)$], as evidenced by the misalignment between the D line and the L line. This observation conclusively verifies the absence of an exceptional point ($E_+=E_-$) under current parameter settings. However, an approximate exceptional point can be identified, where the real parts of E_+ and E_- are equal, $\mathrm{Re}(E_+)=\mathrm{Re}(E_-)$, and the imaginary parts are nearly identical, $\mathrm{Im}(E_+)\approx\mathrm{Im}(E_-)$ (see the black point in Figs. 4(c) and 4(d)).

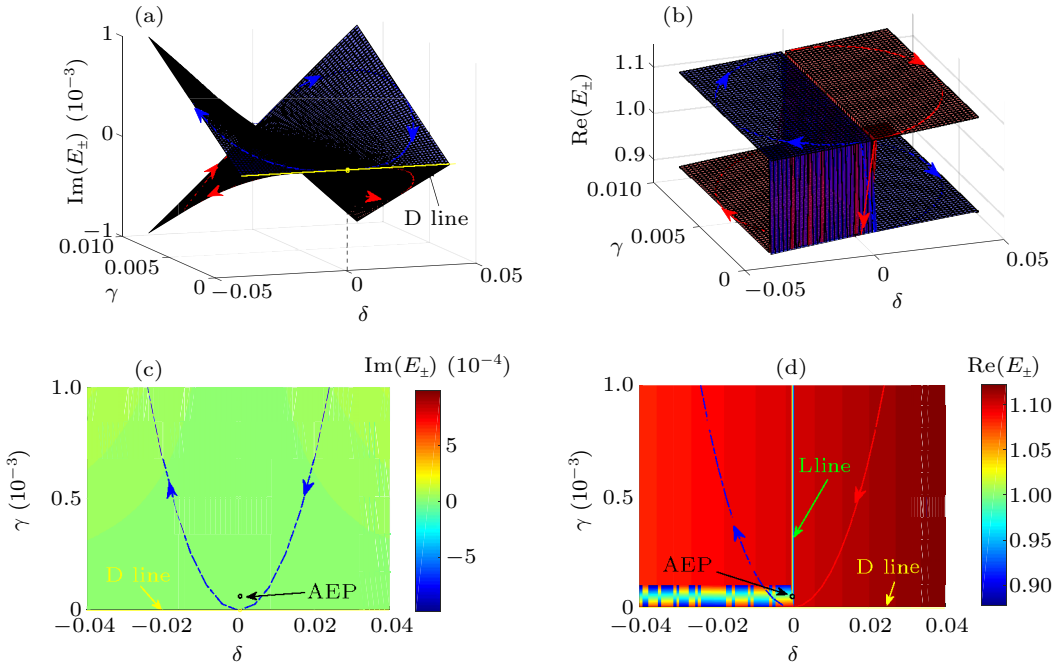


Fig. 4. The eigenenergy spectrum $E_{\pm}(\gamma,\delta)$ and the system time-evolution trajectory $E_{\pm}[\gamma(t),\delta(t)]$ for an asymmetric Bell-state transfer. The imaginary and real parts of the eigenenergy spectrum are shown in panels (a) and (b) as three-dimensional surfaces, while panels (c) and (d) present two-dimensional plots by fixing $\gamma\in(0,0.001)$. The D line and L line indicate the intersection lines of the surfaces corresponding to the imaginary and real parts of $E_{\pm}(\gamma,\delta)$, respectively. The system's time-evolution trajectory dynamically orbits around an AEP, shown as the black point $(0,1\times10^{-4})$ in the parameter space (γ,δ). The other parameters are $g_0=0.1$, $G_0=0$, $\Delta_0=0.04$, $\Gamma_0=0.1$, $\alpha=-1$, and $\omega=\pi$.

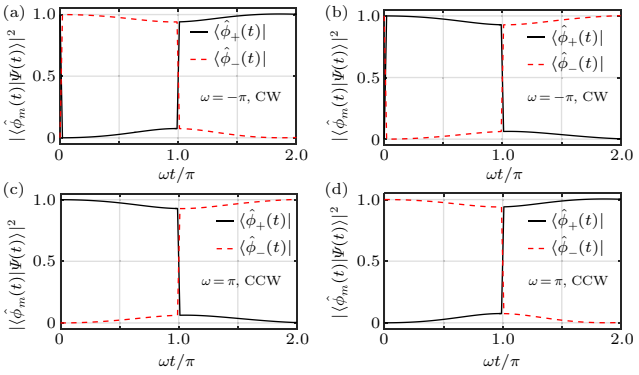


Fig. 5. Time evolution of the fidelity $F_m=|\langle\widehat{\phi_m}(t)|\Psi(t)\rangle|^2$ for the time-dependent right eigenstate $|\phi_m(t)\rangle$ ($m=+,-$). The initial state in panels (a) and (c) [(b) and (d)] is chosen as $|\Psi(0)\rangle=|\phi_+(0)\rangle$ ($|\phi_-(0)\rangle$). The selected trajectories in panels (a)–(b) exhibit clockwise (CW) encircling, while those in panels (c)–(d) demonstrate counterclockwise (CCW) encircling. Other parameters are $g_0=0.1$, $\Delta_0=0.04$, $\Gamma_0=0.1$, and $\alpha=-1$. The state dynamics exhibit chiral behavior, thereby enabling the implementation of an asymmetric Bell-state switch.

According to the conventional notion, the presence of EPs is deemed a prerequisite for the viability of the scheme, suggesting that chiral transformations are unattainable in their absence. However, it is intriguing to observe that even when the system evolves around an AEP, a significant chiral transition still persists. This feasibility stems from the Riemann topology of the system spectrum induced by the AEP and a specific choice of encircling trajectory within the parameter space. Specifically, no exceptional points (EPs) exist in the parameter space (γ,δ) selected in Fig. 4. However, within the broader three-dimensional space (g,γ,δ) or even an N-dimensional space (with N varying parameters), EPs are likely to exist. In such cases, the selected AEP may correspond to one of these neighboring EPs in the high-dimensional space. If the chosen parameter trajectory varies sufficiently slowly around the AEP, asymmetric state transformation can still be achieved.

For example, an asymmetric Bell-state transfer can be attained when the system time-evolution trajectory dynamically orbits around an AEP (see the black point in Fig. 4), in the parameter space (γ,δ). Without loss of generality, the system time-evolution trajectory can be chosen as

$$\delta(t)=\Delta_0\sin(\omega t),\quad \gamma(t)=\Gamma_0\sin^2\left(\frac{\omega t}{2}\right), \tag{10}$$

where Δ_0, Γ_0, and $\omega\in\boldsymbol{R}$ are constants, and the period of the trajectory is $T=2\pi/\omega$. The time-evolution trajectories $E_{\pm}[\gamma(t),\delta(t)]$ are depicted in Fig. 4.

In Fig. 5, we present the temporal evolution of the fidelity for the right eigenstate $|\phi_m(t)\rangle$ ($m=+,-$) under

different initial states and encircling directions. The orbiting trajectory proceeds in a counterclockwise (CCW) or clockwise (CW) direction for positive angular frequencies $\omega > 0$ or negative angular frequencies $\omega < 0$, respectively. As illustrated in Figs. 5(a) and 5(b), the right eigenstates (Bell states) return to their original configurations after completing a dynamical cycle with a CW encircling direction. However, as shown in Figs. 5(c) and 5(d), the Bell states undergo an exchange after completing a dynamical cycle with a CCW encircling direction. The state dynamics thus exhibits a distinct chiral character, facilitating the implementation of an asymmetric Bell-state switch.

4.2. Asymmetric Bell-state transfer under time-independent dissipations

We have demonstrated the realization of chiral Bell-state transfer by modulating time-dependent dissipative parameters. However, it is important to acknowledge that controlling dissipative parameters can be challenging in certain systems or experiments. From an experimental perspective, we propose an alternative approach for achieving chiral Bell-state transfer by employing time-independent dissipative parameters. Furthermore, we present the eigenenergy spectrum $E_\pm$ in the parameter space (g,δ), as shown in Fig. 6. Figure 6(a) demonstrates the separation between the imaginary parts of $E_\pm(g,\delta)$ at the point $(0,0)$, while Fig. 6(b) shows the convergence of the real parts of $E_\pm(g,\delta)$ at the same point. Hence, under the current parameter configuration, the system does not exhibit an EP; instead, it features a distinctive AEP.

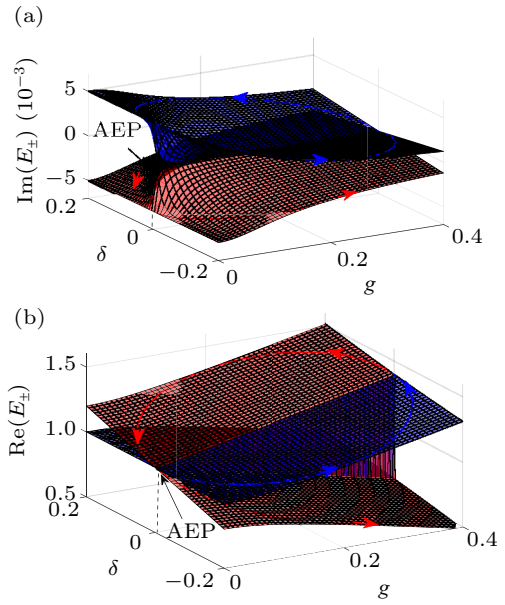


Fig. 6. Eigenenergy spectrum $E_\pm(g,\delta)$ and the system time-evolution trajectory $E_\pm[g(t),\delta(t)]$ for a dissipative system with time-independent dissipation. Panels (a) and (b) show the real and imaginary parts of $E_\pm(g,\delta)$ and $E_\pm[g(t),\delta(t)]$, respectively. The red (blue) Riemann surface corresponds to $E_+(g,\delta)$ $[E_-(g,\delta)]$, and the solid red (dashed blue) line represents $E_+(g,\delta)$ $(E_-(g,\delta))$, respectively. The pink point indicates an AEP. Other parameters are $g_0 = G_0 = \Delta_0 = 0.2$, $\gamma_0 = 0.1$, $\alpha = -1$, and $\omega = \pi$.

The realization of asymmetric Bell-state transfer can be achieved by carefully selecting the parameter trajectory as

$$\begin{aligned} \gamma(t) &= \gamma_0, \quad g(t) = g_0 + G_0\cos(\omega t), \\ \delta(t) &= \Delta_0\sin(\omega t), \end{aligned} \tag{11}$$

where g_0, G_0, γ_0, Δ_0, and $\omega \in \boldsymbol{R}$ are real constants, and the period of the trajectory is $T = 2\pi/\omega$. The time-evolution trajectories of $E_\pm(t)$ are depicted in Fig. 7. It is evident that the trajectories $E_\pm[g(t),\gamma(t)]$ encircle the AEP.

We further present the temporal evolution of the fidelity for the right eigenstates $|\phi_m(t)\rangle$ $(m = +,-)$ under different initial states and encircling directions in Fig. 7. The state dynamics again exhibits a pronounced chiral character, thereby enabling the implementation of an asymmetric Bell-state switch. It is worth noting that the significant state changes observed during the initial stages in Figs. 5(a) and 5(b), as well as Figs. 7(a) and 7(b), arise from deliberately induced nonadiabatic transitions. These transitions are not artifacts, but rather constitute the essential mechanism underpinning the chiral dynamics. The direction of the parameter loop (CW or CCW) determines the timing of these transitions, which in turn dictates whether the system returns to its initial state or evolves into the alternate Bell state upon completion of a full cycle.

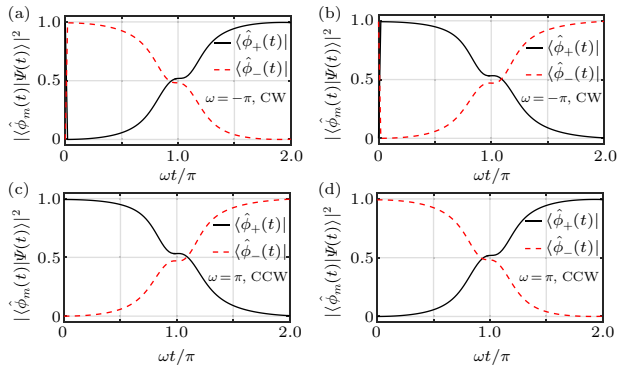


Fig. 7. Time evolution of the fidelity $F_m = |\langle\widehat{\phi_m}(t)|\Psi(t)\rangle|^2$ for the time-dependent right eigenstate $|\phi_m(t)\rangle$ $(m = +,-)$. The initial state in panels (a) and (c) [(b) and (d)] is chosen as $|\Psi(0)\rangle = |\phi_+(0)\rangle$ $(|\phi_-(0)\rangle)$. The trajectory in panels (a)–(b) exhibits clockwise (CW) encircling, while that in panels (c)–(d) exhibits counterclockwise (CCW) encircling. Other parameters are set as $g_0 = G_0 = \Delta_0 = 0.2$, $\gamma_0 = 0.1$, and $\alpha = -1$.

5. Experimental feasibility and conclusion

We briefly discuss the experimental feasibility of the proposed scheme. The required atomic configurations can be implemented using cesium (Cs) or rubidium-87 (^{87}Rb). Trapping atoms inside microwave cavities has been experimentally demonstrated by several research groups,[50,52–63] confirming the practicality of such platforms. The atom–cavity coupling strength g and the detuning δ can be precisely controlled using well-established techniques, as reported in Refs. [53–55]. Moreover, effective dynamic control of the atomic spontaneous emission rate $\gamma(t)$ is experimentally feasible via the

Purcell effect and reservoir-engineering techniques.[56–58] Recent experiments have achieved microwave cavity QED parameters close to those required in our scheme, for example, $(\delta, g, \gamma) \sim 2\pi \times (0, 0.3, 6)$ MHz and $(\delta, g, \gamma) \sim 2\pi \times (24, 24, 12.12)$ MHz.[59–61]

In addition, within our scheme, the atomic spontaneous emission rate γ is chosen to be positive, whereas the effective decay rate κ of the cavity mode can be negative due to its experimental accessibility through gain modulation. Specifically, $\kappa = \kappa_{\text{out}} - \xi$,[48,62] where κ_{out} denotes the intrinsic loss rate of the cavity and ξ represents the externally induced gain (round-trip energy amplification). The sign of κ — positive ($\kappa > 0$, corresponding to net loss) or negative ($\kappa < 0$, corresponding to net gain) — is determined by the relative magnitudes of κ_{out} and ξ. Notably, the regime with $\kappa < 0$ has been extensively investigated theoretically[45,48,62] and has also been realized in recent experimental implementations.[49,63]

In conclusion, we have theoretically demonstrated both symmetric and asymmetric Bell-state transfers in a dissipative Jaynes–Cummings model that incorporates atomic spontaneous emission and cavity decay. For symmetric Bell-state transfer, the detrimental effects of nonadiabatic transitions — originating from the imaginary components of the eigenenergy spectrum — are effectively suppressed through appropriate parameter tuning. Consequently, high-efficiency state transfer can be achieved by selecting a dynamical trajectory that encircles an EP. This enables a long-sought symmetric switching mechanism in which Bell states are dynamically exchanged, independent of the encircling direction. From a topological perspective, the symmetric transfer arises because the eigenstates themselves are exchanged after completion of the parameter loop, as dictated by the topology of the real part of the energy spectrum around the EP.[22,23]

Furthermore, we demonstrate the emergence of chiral dynamics in the dissipative Jaynes–Cummings model without strict reliance on exact exceptional points. In particular, asymmetric Bell-state transfer can be realized even in the absence of a true EP by orbiting around an AEP, where the final state is determined by the orientation of the trajectory. This feature is especially noteworthy. In contrast to conventional approaches that rely on precise EP conditions, our scheme shows that chiral dynamics can be achieved in non-Hermitian systems without stringent requirements on EPs, thereby enabling asymmetric state transfer through dynamical evolution around an AEP. These results significantly reduce the complexity of parameter control and alleviate experimental challenges in non-Hermitian systems with multiple dissipation channels. Finally, we propose an alternative route to chiral Bell-state transfer based on time-independent dissipative parameters.

The results presented in this work have potential applications beyond Bell-state transfer via controlled dissipation, including the coherent transfer of multimode or hybrid entangled states,[64–67] such as Greenberger–Horne–Zeilinger (GHZ) states.[64] Moreover, the realization of transfer protocols involving all four Bell states[41] represents a promising direction for future research. While our theoretical framework is general, the numerical demonstrations presented here are based on specific sinusoidal or cosinoidal time dependences of the system parameters (see Eqs. (8), (10), and (11)). This choice provides a well-defined periodic test case that facilitates a systematic analysis of time-modulated effects. Nevertheless, we acknowledge that practical implementations may involve more complex or even aperiodic temporal modulations. Future work may explore optimal-control strategies for designing time-modulation protocols that maximize entangled-state transfer under realistic experimental constraints and noise environments. Importantly, the general principles identified in this work — particularly the role of modulation timing in realizing symmetric and asymmetric entangled-state transfers — remain applicable to a broad class of modulation schemes beyond the sinusoidal or cosinoidal forms considered here. Overall, our results establish a novel and robust strategy for manipulating entangled states with both symmetric and asymmetric characteristics through dissipation engineering, providing an effective and reliable framework for quantum-state engineering in non-Hermitian systems.

Acknowledgments

This project was supported by the National Key Research and Development Program of China (Grant No. 2024YFA1408900), the National Natural Science Foundation of China (Grant Nos. 12264040, 12374333, and U21A20436), the Jiangxi Natural Science Foundation (Grant Nos. 20232BCJ23022 and 20252BAC240119), the Innovation Program for Quantum Science and Technology (Grant No. 2021ZD0301705), and the Jiangxi Province Key Laboratory of Applied Optical Technology (Grant No. 2024SSY03051).

References

[1] Feng L, El-Ganainy R and Ge L 2017 *Nat. Photon.* **11** 752
[2] Özdemir Ş, Rotter S, Nori F and Yang L 2019 *Nat. Mater.* **18** 783
[3] Heiss W D 2000 *Phys. Rev. E* **61** 929
[4] Cartarius H, Main J and Wunner G 2007 *Phys. Rev. Lett.* **99** 173003
[5] Zhang G Q and You J Q 2019 *Phys. Rev. B* **99** 054404
[6] Zhang G Q, Chen Z, Xu D, Shammah N, Liao M, Li T F, Tong L M, Zhu S Y, Nori F and You J Q 2021 *PRX Quantum* **2** 020307
[7] Peng B, Özdemir Ş K, Lei F, Monifi F, Gianfreda M, Long G L, Fan S, Nori F, Bender C M and Yang L 2014 *Nat. Phys.* **10** 394
[8] Kato T 1995 *Perturbation Theory for Linear Operators* (Berlin: Springer)
[9] Ashida Y, Gong Z and Ueda M 2020 *Adv. Phys.* **69** 249
[10] Wu Q C, Zhao J L, Fang Y L, Zhang Y, Chen D X, Yang C P and Nori F 2023 *Sci. China-Phys. Mech. Astron.* **66** 240312
[11] Zhang S M, He T Y and Jin L 2024 *Chin. Phys. Lett.* **41** 027201

[12] Liu C, Lan J, Gu Z M and Zhu J 2023 *Chin. Phys. Lett.* **40** 124301
[13] Zhang Y X, Zhang Z T, Yang Z S, Wei X Z and Liang B L 2024 *Chin. Phys. B* **33** 060308
[14] Chen W, Abbasi M, Ha B, Erdamar S, Joglekar Y N and Murch K W 2022 *Phys. Rev. Lett.* **128** 110402
[15] Hodaei H, Hassan A U, Wittek S, Garcia-Gracia H, El-Ganainy R, Christodoulides D N and Khajavikhan M 2017 *Nature* **548** 187
[16] Wu Q C, Zhou Y H, Liu T, Kang Y H, Su Q P and Yang C P 2025 *Chin. J. Phys.* **98** 1116
[17] Liu Z P, Zhang J, Özdemir Ş K, Peng B, Jing H, Lü X Y, Li C W, Yang L and Liu Y X 2016 *Phys. Rev. Lett.* **117** 110802
[18] Lin Z, Ramezani H, Eichelkraut T, Kottos T, Cao H and Christodoulides D N 2011 *Phys. Rev. Lett.* **106** 213901
[19] Guo A, Salamo G J, Duchesne D, Morandotti R, Volatier-Ravat M, Aimez V, Siviloglou G A and Christodoulides D N 2009 *Phys. Rev. Lett.* **103** 093902
[20] Bergholtz E J, Budich J C and Kunst F K 2021 *Rev. Mod. Phys.* **93** 015005
[21] Guria C, Zhong Q, Özdemir Ş K, Patil Y S S, El-Ganainy R and Harris J G E 2024 *Nat. Commun.* **15** 1369
[22] Arkhipov I I, Miranowicz A, Minganti F, Özdemir Ş and Nori F 2024 *Phys. Rev. Lett.* **133** 113802
[23] Wu Q C, Zhao J L, Zhou Y H, Ye B L, Fang Y L, Zhou Z W and Yang C P 2025 *Phys. Rev. A* **111** 022410
[24] Khandelwal S, Chen W J, Murch K W and Haack G 2024 *Phys. Rev. Lett.* **133** 070403
[25] Berry M V 2011 *J. Opt.* **13** 115701
[26] Xu H, Mason D, Jiang L and Harris J G E 2016 *Nature* **537** 80
[27] Li A, Dong J, Wang J, Cheng Z, Ho J S, Zhang D, Wen J, Zhang X L, Chan C T, Alù A, Qiu C W and Chen L 2020 *Phys. Rev. Lett.* **125** 187403
[28] Feilhauer J, Schumer A, Doppler J, Mailybaev A A, Böhm J, Kuhl U, Moiseyev N and Rotter S 2020 *Phys. Rev. A* **102** 040201
[29] Ergoktas M S, Soleymani S, Kakenov N, Wang K, Smith T B, Bakan G, Balci S, Principi A, Novoselov K S, Ozdemir S K and Kocabas C 2022 *Science* **376** 184
[30] Arkhipov I I, Miranowicz A, Minganti F, Özdemir Ş and Nori F 2023 *Nat. Commun.* **14** 2076
[31] Hassan A U, Galmiche G L, Harari G and LiKamWa P 2017 *Phys. Rev. A* **96** 052129
[32] Tang Z, Chen T and Zhang X 2023 *Laser Photonics Rev.* **18** 2300794
[33] Hassan A U, Zhen B, Soljačić M, Khajavikhan M and Christodoulides D N 2017 *Phys. Rev. Lett.* **118** 093002
[34] Tang X, Chen T and Zhang X D 2025 *Phys. Rev. Research* **7** 013159
[35] Zhang X L, Jiang T and Chan C T 2019 *Light Sci. Appl.* **8** 88
[36] Nasari H, Galmiche G L, Aviles H E L, Schumer A, Hassan A U, Zhong Q, Rotter S, LiKamWa P, Christodoulides D N and Khajavikhan M 2022 *Nature* **605** 256
[37] Verstraete F, Wolf M M and Cirac J I 2009 *Nat. Phys.* **5** 633
[38] Wu Q C, Zhou Y H, Ye B L, Liu T and Yang C P 2021 *New J. Phys.* **23** 113005
[39] Zou J, Zhang S and Tserkovnyak Y 2022 *Phys. Rev. B* **106** 180406
[40] Schine N, Young A W, Eckner W J, Martin M J and Kaufman A M 2022 *Nat. Phys.* **18** 1067
[41] Tang Z, Chen T, Tang X and Zhang X D 2024 *Light Sci. Appl.* **13** 167
[42] Shore B W and Knight P L 1993 *J. Mod. Opt.* **40** 1195
[43] Bishop L S, Ginossar E and Girvin S M 2010 *Phys. Rev. Lett.* **105** 100505
[44] Minganti F, Miranowicz A, Chhajlany R W, Arkhipov I I and Nori F 2020 *Phys. Rev. A* **101** 062112
[45] Naghiloo M, Abbasi M, Joglekar Y N and Murch K W 2019 *Nat. Phys.* **15** 1232
[46] Zhou Y H, Shen H Z, Zhang X Y and Yi X X 2018 *Phys. Rev. A* **97** 043819
[47] Liu C and Huang J F 2024 *Sci. China-Phys. Mech. Astron.* **67** 240312
[48] Li J, Yu R and Wu Y 2015 *Phys. Rev. A* **92** 053837
[49] Feng L, Wong Z J, Ma R M, Wang Y and Zhang X 2014 *Science* **346** 972
[50] Chen W, Özdemir Ş, Zhao G, Wiersig J and Yang L 2017 *Nature* **548** 192
[51] Arkhipov I I, Miranowicz A, Nori F, Özdemir Ş K and Minganti F 2023 *Phys. Rev. Res.* **5** 043092
[52] Khudaverdyan M, Alt W, Kampschulte T, Reick S, Thobe A, Widera A and Meschede D 2009 *Phys. Rev. Lett.* **103** 123006
[53] Leibfried D, Blatt R, Monroe C and Wineland D 2003 *Rev. Mod. Phys.* **75** 281
[54] Miroshnychenko Y, Alt W, Dotsenko I, Förster L, Khudaverdyan M, Meschede D and Rauschenbeutel 2006 *Nature* **442** 151
[55] Trupke M, Hinds E A, Eriksson S, Curtis E A, Moktadir Z, Kukharenka E and Kraft M 2005 *Appl. Phys. Lett.* **87** 211106
[56] Mizuno K, Pae J, Nozokido T and Furuya K 1987 *Nature* **328** 45
[57] Breuer H P and Petruccione F 2007 *The Theory of Open Quantum Systems* (Oxford: Oxford University Press)
[58] Kienzler D, Lo H-Y, Keitch B, de Clercq L, Leupold F, Lindenfelser F, Marinelli M, Negnevitsky V and Home J P 2015 *Science* **347** 53
[59] Yang P, Xia X, He H, Li S, Han X, Zhang P, Li G, Zhang P, Xu J, Yang Y and Zhang T 2019 *Phys. Rev. Lett.* **123** 233604
[60] Wang J, Huang D Y, Zhou X L, Shen Z M, He S J, Huang Q Y, Liu Y J, Li C F and Guo G C 2025 *Phys. Rev. Lett.* **134** 240802
[61] Steck D A Rubidium 87 D line data available online at http://steck.us/alkalidata
[62] Xing Y, Qi L, Cao J, Wang D Y, Bai C H, Wang H F, Zhu A D and Zhang S 2017 *Phys. Rev. A* **96** 043810
[63] Hodaei H, Miri M A, Heinrich M, Christodoulides D N and Khajavikhan M 2014 *Science* **346** 975
[64] Wu Q C, Zhou Y H, Ye B L, Liu T, Zhao J L, Chen D X and Yang C P 2022 *Ann. Phys.* **534** 2100393
[65] Zheng X W, Zheng J C, Pan X F, Lin L H, Han P R and Li P B 2025 *Phys. Rev. A* **111** 012402
[66] Liu B B, Su S L, Zuo Y L, He Q, Chen G, Nori F and Jing H 2024 arXiv: 2407.08525
[67] Feyisa C G, You J S, Ku H Y and Jen H H 2025 *Quantum Sci. Technol.* **10** 025021